

****FULL TITLE****
ASP Conference Series, Vol. ****VOLUME****, ****YEAR OF PUBLICATION****
****NAMES OF EDITORS****

How Compact are the Cores of AGN ? Sub-Parsec Scale Imaging with VLBI at Millimeter Wavelength

T.P. Krichbaum¹, S.S. Lee¹, A.P. Lobanov¹, A.P. Marscher², M.A. Gurwell³

¹*Max-Planck-Institut für Radioastronomie, Bonn, Germany*

²*Institute for Astrophysical Research, Boston University, Boston, MA 02215, USA*

³*Harvard-Smithsonian Center for Astrophysics, Cambridge, MA 02138, USA*

Abstract. We study the most central regions of AGN jets with an angular resolution of tens of micro-arcseconds using VLBI at millimeter wavelengths (mm-VLBI). We present and discuss a new 86 GHz VLBI survey of compact radio sources. We show new high dynamic range images of two nearby radio galaxies (3C 120 and M87). In M87 the size of the compact VLBI core (the jet base) is < 15 Schwarzschild radii. Future mm-VLBI observations at 1 mm and shorter wavelengths should lead to images of galactic and extragalactic radio sources with a spatial resolution down to a few Schwarzschild radii of the central super massive black holes. To achieve this, the participation of large and sensitive millimeter and sub-millimeter telescopes in VLBI is essential.

1. Introduction and Scientific Motivation

Radio galaxies and quasars produce powerful relativistic plasma jets, accelerating particles up to TeV energies. Jets are not unique to AGN, but are also observed in other objects like in X-ray binaries, micro-quasars, young stellar objects and probably also in Gamma-ray bursters. In modern theory, the launching and acceleration of the relativistic jets is explained via MHD processes, with magnetic fields either attached to the rotating accretion disk or directly linked to the ergosphere of the central and possibly rotating super-massive black hole (e.g. Narayan 2005).

In order to better understand the process of jet formation, a study of the inner most regions of compact radio sources is necessary. VLBI at short millimeter wavelengths (mm-VLBI) provides, via its unrivaled angular resolution of only a few ten micro-arcseconds (at $\lambda = 1$ mm), an almost unique tool to test and discriminate between the different theoretical models. In addition to the high spatial resolution (corresponding to ≤ 10 Schwarzschild radii for nearby sources like Sgr A* or M87), the high observing frequency allows to image emission regions, which are self-absorbed and therefore not observable at longer wavelengths.

In the following we present some results from global 3 mm-VLBI performed with the Global Millimeter VLBI Array (GMVA¹) at 86 GHz. VLBI observations

¹see: <http://www.mpifr-bonn.mpg.de/div/vlbi/globalmm/index.html>

Author	Ant.	Sensitivity	Number	Detections
Beasley et al. 1997	3	~ 0.5	N=45	16%
Lonsdale et al. 1998	3-5	~ 0.7	N=79	14%
Rantakyro et al. 1998	6-9	~ 0.5	N=67	24%
Lobanov et al. 2000	3-5	~ 0.4	N=28	93%
Lee et al. 2008	12	~ 0.2	N=127	95%

Table 1. VLBI surveys at 86 GHz: Col.1 gives the reference, col.2 the number of antennas, col.3 the typical detection sensitivity (7σ) in [Jy], col.4 the number of observed sources and col.5 the percentage of detected objects (detection rate).

at shorter wavelengths ($\lambda < 3$ mm, $\nu > 100$ GHz) are possible but are still limited by the number of available mm-telescopes (typically $N \leq 3 - 4$), their sensitivity and the limited observing bandwidth (see e.g. Krichbaum et al. 2007, and references therein). To date, it is therefore not yet possible to produce a reliable map of a radio source at these shorter wavelengths. The GMVA combines the sensitive and mm-capable telescopes in Europe (100 m Effelsberg, 6x15 m Plateau de Bure, 30 m Pico Veleta, 20 m Onsala, & 14 m Metsähovi) with the VLBA. The GMVA is open to the scientific community and calls for observing proposals twice per year (proposal deadlines: Feb. 1st, Oct. 1st). It enables imaging of compact radio sources at an angular resolution of $\gtrsim 40\mu\text{as}$. The transatlantic detection sensitivity (7σ) ranges between $\sim (80 - 200)$ mJy on the most sensitive baselines (for 512 Mbps). This should be compared with the $\sim (300 - 400)$ mJy baseline sensitivity of the stand-alone VLBA. In a typical 12 hr GMVA observing run, an image rms of $\sigma_{\text{map}} \lesssim (1 - 4)$ mJy is reached.

2. A New and Comprehensive 86 GHz VLBI Survey

VLBI surveys at the highest possible frequency and resolution are important for answering questions on the compactness of extragalactic radio sources, systematic differences between source classes, and if and how the brightness temperature varies along the jet and towards the region, where the jet is made. The latter is closely related to observational tests of jet launching models. Due to the limited sensitivity of early 3 mm-VLBI and the relatively small number of telescopes, previous surveys revealed only moderately low ($\leq 20 - 30\%$) detection rates and small numbers of observable sources. Table 1 summarizes the existing 3 mm VLBI surveys in chronological order.

After more sensitive VLBI telescopes became available around year 2000, a new and larger than previous VLBI snap-short survey was conducted. The observations took place in 3 sessions (October 2001, April & October 2002), with the participation of the VLBA (8 antennas), Haystack, Pico Veleta, Plateau de Bure, Effelsberg, Onsala and Metsähovi. Mainly due to the high sensitivity of the IRAM telescopes, a detection sensitivity of $\sim (0.2 - 0.3)$ Jy could be reached. This resulted in an impressive detection rate of 95%, which equals to detection of 121 out of 127 observed sources, of which 109 objects (86%) could be imaged (see Table 1) (Lee et al. 2007; Lee 2008).

After fitting of Gaussian components to the visibility data for each source, the flux, position and size (FWHM) of the VLBI components were measured. In Figure 1 we plot the resulting distribution of the measured core flux densities (top left) and sizes (bottom left) for Quasars, BL-Lacertae Objects, Radio-

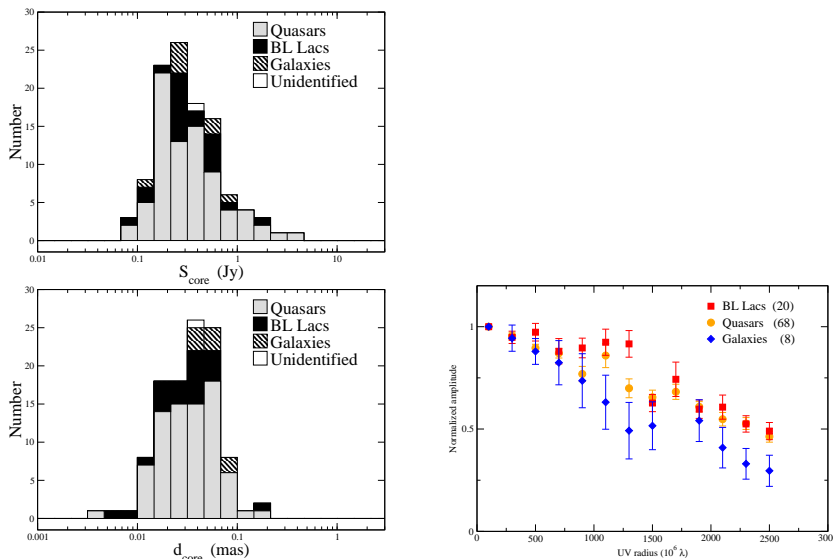


Figure 1. Distribution of flux density (top left) and angular size (bottom left) of the core components for the survey. The shading denotes different object classes. Left: Binned, averaged and normalized visibility amplitude plotted versus uv-distance. Different symbols identify the different object types. Numbers in brackets give the number of objects in each class. Some visibility bins (interval: $200 M\lambda$) do not contain data for each source class (Lee 2008).

Galaxies and the unidentified objects. The right panel of Figure 1 shows the mean normalized visibility amplitudes of the optically identified sources.

3. The inner jet of 3C 120

In Figure 2 we show a 43 GHz VLBA map and a 86 GHz GMVA map of the radio galaxy 3C 120, observed in October 2004. The left panel shows uv-tapered maps convolved with a (0.1×0.3) mas beam. The right panel shows the un-tapered central 0.5 mas region of the jet, convolved with the smaller 86 GHz beam (0.06×0.25 mas). At the redshift of 3C 120 ($z = 0.033$) an angular scale of 1 mas corresponds to a spatial scale of 0.63 pc. Assuming negligible variability on the 16 day interval between the two observing dates, it is possible to determine the spectral indices $\alpha_{43/86\text{GHz}}$ along the jet ($S \propto \nu^\alpha$). For the labeled regions A to F in Figure 2 (left), we obtain spectral indices of -0.35 for A ($r = 0$ mas), -0.07 for B ($r = 0.1$ mas), -0.36 for C ($r = 0.25 - 0.4$ mas), -0.46 for D ($r = 0.8$ mas), -0.7 for E ($r = 1.2$ mas) and -0.8 for F ($r = 1.8 - 2.2$ mas). A general trend of spectral steepening with increasing core separation is obvious. We note that component B exhibits a much flatter spectrum than the core component A. With a size of ~ 0.1 mas (FWHM) and a spectral turnover frequency ($43 \leq \nu_m \leq 86$) GHz, component B cannot be in energy equipartition, and is dominated by the magnetic field energy. Similar arguments for the core region (component A, size $\leq 32 \mu\text{as} \leq 7 \cdot 10^{16}$ cm) and for the outer jet components (C–F) yield no evidence for a substantial deviation from equipartition. The higher angular resolution at 86 GHz (Fig. 2, right) also reveals some structural difference to

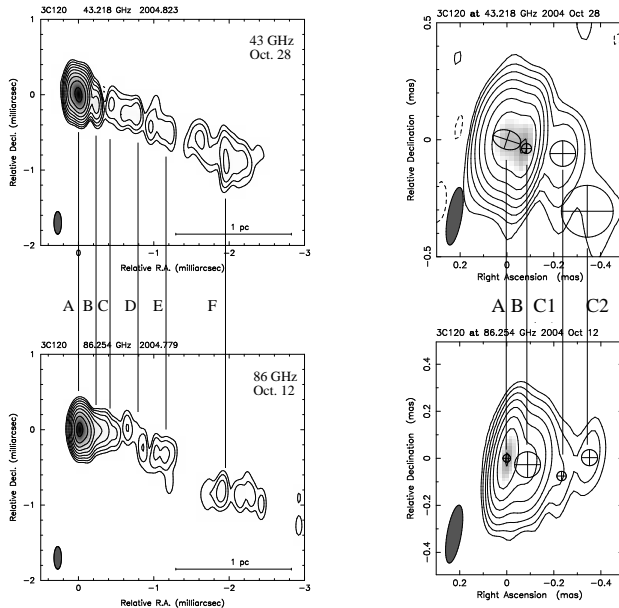


Figure 2. VLBI maps of 3C 120 at 43 GHz (top, VLBA: Oct. 28, 2004) and 86 GHz (bottom, GMVA: Oct. 16, 2004). The maps result from a reanalysis of previously published data (Marscher et al. 2007). The uv-tapered maps on the left show a faint and partially resolved one sided jet extending to at least $r \sim 2$ mas. On the right, the central 0.5 mas region is shown with higher angular resolution (beam: (0.06×0.25) mas). Lines and labels guide the eye and help to identify corresponding emission regions. Circles in the contour maps on the 2 right panels show size and position of Gaussian components fitted to the visibility data. At 86 GHz, the core size is $\leq 32 \mu\text{as}$.

the 43 GHz map. Remarkable is the difference in the position angle of the inner ($r < 0.5$ mas) jet components. This could be interpreted as evidence for transverse jet stratification.

4. 3C 454.3 after a major outburst in 2005:

In May-June 2005, the quasar 3C 454.3 ($z = 0.859$) showed a major flux density outburst, which was observed from hard X-ray to radio bands (e.g. Villata et al. 2007, and references therein). The flux variations at 1.3 mm and 0.85 mm are shown in Figure 3 (top, right). During the flare maximum quasi-periodic oscillations on a ~ 11 day time scale appear, possibly indicating motion in a helical jet with ~ 100 Schwarzschild radii diameter (assuming $M_{\text{BH}} = 10^9 M_{\odot}$). A Doppler-boosting factor of $\delta \simeq 5 - 9$ would be necessary to bring the observed variability brightness temperature of $T_B \simeq 10^{14}$ K (at 230 GHz) back to the inverse Compton limit of $\sim 10^{12}$ K. The spectral evolution of the flare through the radio bands is shown in Figure 3 (bottom, left). It is obvious that the variability is most pronounced at short mm-wavelengths, with a spectral turnover moving from initially $\simeq 230$ GHz to lower frequencies. Below ~ 10 GHz almost no variability is seen.

So far, VLBI observations at frequencies $\nu \leq 43$ GHz did not reveal strong evidence for the ejection of a new jet component, which could be related to this

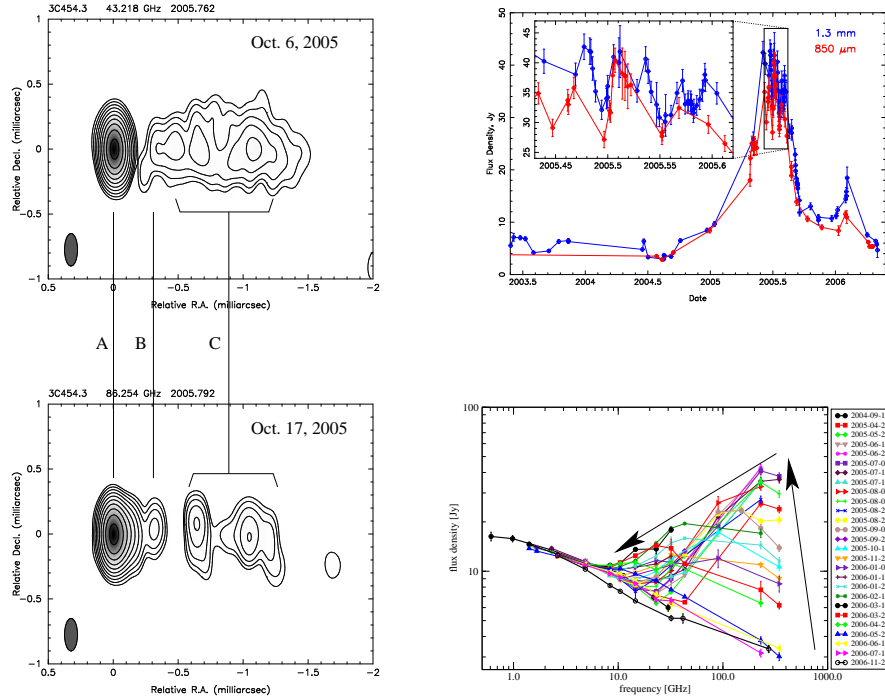


Figure 3. Left: 43 GHz VLBA (top, data from Marscher et al.) and 86 GHz GMVA (bottom) map of 3C 454.3 observed in Oct. 6 and Oct. 17, 2005. Both maps are restored with a common beam of (0.1×0.25) mas. Lines with labels connect the three corresponding emission regions A, B and C (see text). Top right: Flux density variability at 230 and 345 GHz. The insert shows the variability during the time of the peak flux (data: SMA, Gurwell et al. 2007). Bottom right: Evolution of the radio spectrum of 3C 454.3 after the optical flare. The spectra cover a time range from Sep. 2004 until Nov. 2006 at time intervals of a few weeks. The arrows mark the direction of spectral evolution. Each spectrum is obtained from quasi-simultaneous flux measurements, combining data from Effelsberg, VLA, IRAM, SMA & Ratan-600.

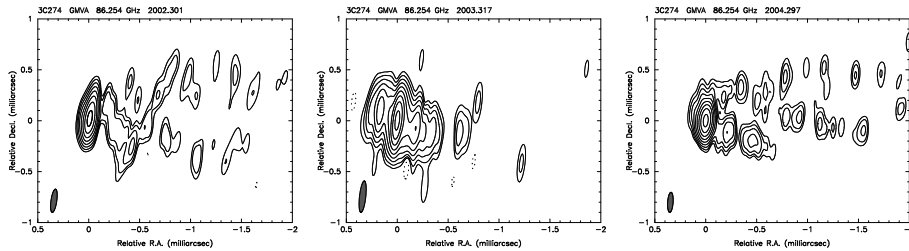


Figure 4. 86 GHz VLBI images of M 87 (3C 274) obtained with global 3 mm VLBI in April 2002, 2003, and 2004 (from left to right). The contour levels are at $-0.3, 0.3, 0.6, 1.2, 2.4, 4.8, 9.6, 19.2, 38.4,$ and 76.8% of the peak flux, of 0.52 Jy/beam (2002), 0.73 Jy/beam (2003), 0.35 Jy/beam (2004). The lowest contour level is omitted in the image of 2002. The restoring beam sizes are 0.23×0.057 mas (2002), 0.31×0.062 mas (2003), and 0.20×0.054 mas (2004), respectively.

flare. In Figure 3 (left panel) we show two VLBI maps obtained about 4 months after the flare. The 86 GHz data reveal a clear elongation of the core region A, which is not visible in the 43 GHz map (region B). A spectral index calculation for the three main emission regions yields for the core A $\alpha_{43/86\text{GHz}} = -0.4$, for the region B $\alpha = +(1.1\dots 2.6)$ and for the jet C $\alpha = -0.3$. The strongly inverted spectrum of the region B indicates possible fore-ground absorption, perhaps from a cloud or torus. With a radial extent ranging from $r_{\text{min}} \lesssim 0.1$ mas to $r_{\text{max}} \simeq 0.3$ mas (0.1 mas corresponds to 0.75 pc) and a sufficiently high opacity, the inner portion of the jet would become visible only at the highest frequencies.

5. The Jet of M 87

In Figure 4 we show 3 images of the inner jet in M 87 (3C 274) obtained with the GMVA at 86 GHz during 2002-2004. The map of 2004 has a higher dynamic range than the earlier images due to increased observing bandwidth (512 Mbps). To our knowledge, these are the highest angular and spatial resolution maps ever made of this source. At a distance of $D=16.75$ Mpc, the minor axis of the GMVA observing beam of $\sim 54\mu\text{as}$ translates into a spatial scale of $1.35 \cdot 10^{16}$ cm (4.4 mpc). From the slightly elliptical observing beam one obtains a formal upper limit for the core size of $\leq (200 \times 54) \mu\text{as}$, which corresponds to $R_s=(56 \times 15)$ Schwarzschild radii (for $M_{BH} = 3 \cdot 10^9 M_\odot$). We may identify the size of the brightest and most compact VLBI component with the jet diameter at or near its origin. In this case it is remarkable that the jet base is so small and bright ($T_B \geq 2 \cdot 10^{10}$ K), contrary to expectations from magnetic-slingshot type acceleration models (e.g. Blandford & Payne 1982). Here, magnetic fields are anchored in the rotating accretion disk, expand and form a light-cylinder. Its diameter defines the minimum jet width of $> 50R_s$ (Camenzind 1990; Fendt & Memola 2001). The observed small size therefore points more towards models in which the jet is attached more directly to the rotating black hole (Blandford & Znajek 1977), gaining its energy via MHD interaction with the inner disk (e.g. Mc Kinney 2006) or the Penrose process (Gariel et al. 2007, and references therein).

The images of 2002 and 2004 both show a bifurcated conically opening one-sided jet, similar to the jet morphology seen at 43 GHz (Walker et al., this conference). The transverse width of the jet is of order of $0.5 - 0.7$ mas, corresponding to a jet diameter of $\sim 140 - 200$ Schwarzschild radii (at $r = 0.5 - 2$ mas core separation). There are clear signs of edge-brightening and a ‘hollow’ or at least faint central jet body. We note that for a jet inclination $> (30 - 45)^\circ$, a fast jet spine could be Doppler-deboosted and remain faint.

In 2003, a component located ~ 0.2 mas east of a ~ 4 times brighter and more compact component is seen. At present it is unclear, if this eastern component should be identified with the jet base (which then must vary in compactness), or if the eastern component is part of a counter-jet. In any case, the structural differences between the 3 maps (and in the corresponding visibility data) indicate pronounced jet variability on and below the 1 year timescale. For the variations with an angular rate ≥ 0.2 mas/yr the corresponding jet speed would be $\beta_{\text{app}} > 0.05$. More frequent global 3mm-VLBI observations are required to follow this motion.

6. VLBI at shorter wavelengths and Future Outlook

After the successful detection of a number of radio source on continental and on transatlantic VLBI baselines at 129, 147 and 230 GHz (see Krichbaum et al. 2007, and references therein), the technical feasibility of VLBI at wavelengths shorter than 3 mm has now been demonstrated. In the next step, and after upgrade of the existing VLBI data acquisition systems to higher data rates of $\sim 2 - 4$ Gbps and observing bandwidths of ≥ 512 MHz, the baseline sensitivity will dramatically improve ($\lesssim 0.5$ Jy at 230 GHz for the existing antennas). With a relatively small VLBI array consisting of $N = 2 - 4$ mm-telescopes, a systematic VLBI survey of the degree of compactness of a large sample of radio sources could be tackled. The further addition of more and more sensitive mm-capable telescopes (see Table 2), will lead to true imaging capability². Such effort appears justified, since the VLBI imaging of the Galactic Center source Sgr A*, M87 and other nearby objects at 230 and 345 GHz will allow to map the direct vicinity of super massive black holes with a spatial resolution of $\leq 5 - 6$ Schwarzschild radii ! In this context, the participation of the large and sensitive millimeter interferometers (SMA, PdB, CARMA, ALMA) and large single dish telescopes (e.g the LMT) is essential, not only for reaching a high detection sensitivity, but also for providing a dense uv-coverage. Only with the latter an image fidelity can be reached, which in the end might allow to directly observe the expected image distortions and General Relativity effects in the vicinity of a black hole.

References

- Beasley, A.J., Dhawan, V., Doeleman, S., & Phillips, R.B. 1997, Millimeter-VLBI Science Workshop, ed. R. Barvainis & R.B. Phillips, Haystack Obs., p. 53
- Blandford, R.D., & Payne, D.G. 1982, MNRAS, 199, 883
- Blandford, R.D., & Znajek, R.L. 1977, MNRAS, 179, 433
- Camenzind, M. 1990, RvMA, 3, 234
- Fendt, C. & Memola, E. 2001, A&A, 365, 631
- Gariel, J., et al. 2007, in press (arXiv:gr-qc/0702123v1)
- Gurwell, M., et al. 2007, in: 'From Z-Machines to ALMA: (Sub)millimeter Spectroscopy of Galaxies', eds. A. J. Baker et al., ASP Conference Series, in press
- Krichbaum, T.P., Agudo, I., Bach, U., Witzel, A., Zensus, J.A., in: 'New Developments in VLBI Science and Technology', 8th EVN Symposium, ed. A. Marecki et al., Torun Observatory, Poland, 2007, in press (astro-ph/0611288)
- Lee, S.S., et al. 2007, in: in: 'New Developments in VLBI Science and Technology', 8th EVN Symposium, ed. A. Marecki et al., Torun Observatory, Poland, 2007, in press
- Lee, Sang-Sung, 2008, Phd Thesis, Bonn University
- Lobanov, A.P., et al. 2000, A&A, 364, 391
- Lonsdale, C.J., Doeleman, S.S., & Phillips, R.B. 1998, AJ, 116, 8
- Marscher, A.P., Jorstad, S.G., Gomez, J.L., et al. 2007, ApJ, 665, 232
- McKinney J.C. 2006, MNRAS368, 1561
- Narayan, R., 2005, New Journal of Physics, 7, 199
- Rantakyro, F.T., et al. 1998, A&AS, 131, 451
- Villata, M., et al. 2007, A&A, 464, L5

²At least 4-5 stations are needed for hybrid mapping; the image quality increases with the number of VLBI telescopes.

Name	Country	D [m]	Alt. [m]	Surf. [μm]	90 [GHz]	150 [GHz]	230 [GHz]	345 [GHz]
Surface < 50 μm								
SMA	HI, USA	8x6	4100	12	-	-	+	+
HHT-SMTO	AZ, USA	10	3100	15	-	V	V	+
APEX	Chile	12	5000	18	-	-	+	+
ASTE	Chile	10	4800	20	-	?	?	+
CSO	HI, USA	10	4100	25	-	?	+	+
JCMT	HI, USA	15	4100	25	-	?	V	+
Surface 50 – 100 μm								
Pl.de Bure	France	6x15	2550	55	V	+	V	+
Pico Veleta	Spain	30	2900	67	V	V	V	+
CARMA	CA, USA	^a	2200	30-60	+	?	V	+
Kitt Peak	AZ, USA	12	2000	75	V	V	+	-
Surface 100 – 300 μm								
Metsahovi	Finland	14	sea l.	100	V	V	-	-
Mopra	Australia	22	900	\sim 120	+	-	-	-
Onsala	Sweden	20	sea l.	130	V	?	-	-
VLBA	USA	25	^b	150	V	?	-	-
Taeduk	Korea	14	200	170	+	?	-	-
Nobeyama	Japan	45	1300	200	+	+	-	-
Cambridge	UK	32	20	200	?	-	-	-
Haystack	MA, USA	37	150	250	V	-	-	-
Delingha	China	14	3200	250	+	-	-	-
Simeiz	Ukraine	22	sea l.	250	?	-	-	-
Surface 300 – 500 μm								
GBT	VA, USA	100	840	390 ^c	+	-	-	-
Noto	Italy	32	30	400	+	-	-	-
Effelsberg	Germany	100	300	450	V	-	-	-
under construction								
ALMA	Chile	50x12	5000	25	+	+	+	+
LMT	Mexico	50	4600	70	+	+	+	+
Haystack ^d	MA, USA	37	150	100	+	?	-	-
Yebes	Spain	40	850	150	+	?	-	-
KVN	Korea	3x21	200	\sim 150	+	?	-	-
SRT	Italy	64	600	\sim 200	+	?	-	-

Notes:

^a: inhomogeneous array (6x10m+9x6m)^b: 10 different antennas with elevations ranging from sea level to 4100 m^c: present value, aim is \sim 210 μm ^d: after upgrade

Table 2. Antennas for mm-VLBI, present status and future candidates. Col. 3 gives the antenna diameter, col. 4 the altitude, col. 5 the surface rms. Columns 6-9 summarize the suitability for mm-VLBI at a given observing band, with the following symbols: "V" : VLBI successfully done, receiver available; "+" : in principle possible, receiver available or planned; "?" : perhaps possible, but presently no receiver; "-" : not possible, surface not good enough.